Nonmagnetic impurity perturbation to the quasi-two-dimensional quantum helimagnet $LiCu_2O_2$

H. C. Hsu,[1,2] J.-Y. Lin,[3] W. L. Lee,[4] M.-W. Chu,[1] T. Imai,[5,6] Y. J. Kao,[7] C. D. Hu,[7] H. L. Liu,[2] and F. C. Chou[1,8,*]

[1]*Center for Condensed Matter Sciences, National Taiwan University, Taipei 10617, Taiwan*

[2]*Department of Physics, National Taiwan Normal University, Taipei 116, Taiwan*

[3]*Department of Physics, National Chiao Tung University, HsinChu 30076, Taiwan*

[4]*Institute of Physics, Academia Sinica, Taipei 11529, Taiwan*

[5]*Department of Physics, McMaster University, Ontario, Canada L8S 4M1*

[6]*Canadian Institute for Advanced Research, Toronto, Ontario, Canada M5G1Z8*

[7]*Department of Physics, National Taiwan University, Taipei 10617, Taiwan*

[8]*National Synchrotron Radiation Research Center, HsinChu 30076, Taiwan*

(Received 10 July 2010; revised manuscript received 2 September 2010; published 29 September 2010)

A complete phase diagram of Zn-substituted quantum quasi-two-dimensional helimagnet $LiCu_2O_2$ has been presented. Helical ordering transition temperature (T_h) of the original $LiCu_2O_2$ follows finite size scaling for less than ~5.5% Zn substitution, which implies the existence of finite helimagnetic domains with domain boundaries formed with nearly isolated spins. Higher Zn substitution $\geq$5.5% quenches the long-range helical ordering and introduces an intriguing Zn-level-dependent magnetic phase transition with slight thermal hysteresis and a universal quadratic field dependence for $T_c(\mathrm{Zn}>0.055,\mathrm{H})$. The magnetic coupling constants of nearest-neighbor J_1 and next-nearest-neighbor J_2 ($\alpha=J_2/J_1$) are extracted from high temperature series expansion fitting and $N=16$ finite chain exact diagonalization simulation. We have also provided evidence of direct correlation between long-range helical spin ordering and the magnitude of electric polarization in this spin-driven multiferroic material.

DOI: 10.1103/PhysRevB.82.094450 PACS number(s): 75.10.Pq, 75.40.−s, 75.50.Lk, 75.60.−d

I. INTRODUCTION

$LiCu_2O_2$ is a complex spin-driven multiferroics which shows spontaneous electric polarization below the spin spiral ordering temperature near 22 K.[1] The noncollinear spiral spin structure allows inversion symmetry breaking and manifested a finite electric polarization. The nature of helimagnetic ordering and its correlation to the existence of electric polarization has been the central topic in the research of multiferroics. In particular, microscopic model based on spin supercurrent or inverse Dzyaloshinskii-Moriya interaction provided the theoretical ground for the generation of electric polarization $\mathbf{P}$ within noncollinear magnets, i.e., $\mathbf{P}\propto\mathbf{Q}\times(\mathbf{S}_i\times\mathbf{S}_j)$, where $\mathbf{Q}$ is the cycloidal vector pointed from neighboring spin sites i to j.[2–4] Incommensurate helimagnetic ordering has been found in $LiCu_2O_2$ and accompanies weak electric polarization of multiferroic nature although conflicting results on the cycloidal spin plane assignment and disagreement between experimental ferroelectric properties and spin-current model predictions remain.[1,3–7]

$LiCu_2O_2$ has a Cu-O chain structure formed with edge-sharing CuO_4 plaquettes in the ab plane while these chains are connected through CuO_2 dumbbells along the c direction as shown in Fig. 1.[10] This compound is uniquely composed of nearly equal amount of Cu^+ and Cu^{2+} with Cu^+ sitting in the O-Cu-O dumbbell (along the c direction) to connect the nearest-neighbor edge-sharing spin chains. Undoped $LiCu_2O_2$ shows a helical spin ordering below ~22 K, as indicated by the $d\chi/dT$ peaks, which has been verified by magnetic neutron-scattering studies before.[3,4] Two $d\chi/dT$ peaks occur near ~22 and 24 K, which are anisotropic and more pronounced for magnetic field applied $\|ab$ and $\|c$, respectively. Between 22–24 K, spins have been described as collinear and sinusoidal structure with spin direction along c axis according to ^{7}Li-NMR studies.[11] The anisotropic magnetic correlation lengths ξ_{ab} and ξ_c have been extracted using synchrotron resonant soft x-ray magnetic scattering. It is suggested that the transitions near ~24 and 22 K correspond to the quasi-two-dimensional (quasi-2D) short-range and the following three-dimensional long-range orderings, respectively.[3,12] Li deficiency is proposed to introduce spin-1/2 Cu^{2+} to the bridging spinless Cu^+ site and the helimagnetic ordering temperature is reduced only slightly from ~22 to 20 K for samples nearly free of Li deficiency.[13]

Many early works attempted to describe $LiCu_2O_2$ as an alternating Heisenberg antiferromagnetic chain and applied Bonner-Fisher fitting to the magnetic susceptibility for $T>T_h$; however, the fitting is generally unsatisfactory.[14,15] Later nearest-neighbor (nn) exchange coupling J_1 is found to be ferromagnetic and J_2 to be antiferromagnetic, based both on local-density approximation (LDA) calculation and neutron-scattering spin-wave analysis, which satisfies the classical spin spiral ordering requirement of $|J_2/J_1|>\frac{1}{4}$ as verified experimentally.[8,9] Quantum fluctuation must sustain in the spin spiral ordered state to account for the discrepancy found in polarized neutron-scattering intensity for this frustrated low-dimensional spin-1/2 system.[3]

If we assign the shortest Cu-Cu distance within the edge-sharing chain to be the J_1, its Cu-O-Cu bond angle of ~94° is expected to be ferromagnetic interaction, following the Goodenough-Kanamori-Anderson rule, as summarized in Fig. 2.[16–18] There have been two major views on assigning spin chains and its interchain coupling before, one simply viewing the edge-shared CuO_4 network as linear spin chains shown in Fig. 1(b),[1,19] and the other connecting the Cu between linear CuO_2 chains to form zigzag chain described by

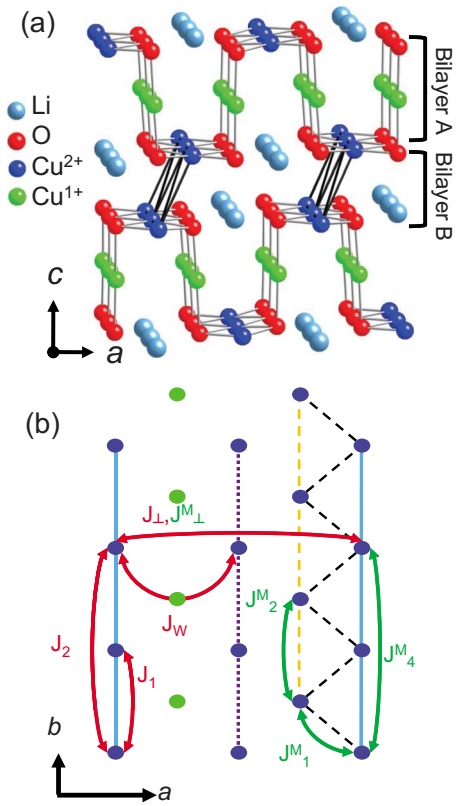

FIG. 1. (Color online) (a) Crystal structure of $LiCu_2O_2$. (b) Magnetic couplings described by linear chain model and zigzag chain model. The purple dot line represents the upper chain within layer A. The orange dashed line represents the lower chain within bilayer B. Linear chain model is adapted from Gippius *et al.* (Ref. 8) and zigzag chain model is adapted from Masuda *et al.* (Ref. 9) distinguished with superscript M. Note the J_W is defined as superexchange coupling between upper and lower Cu^{2+} in bilayer A bridged by the zigzag shape channel through Cu^{+}.

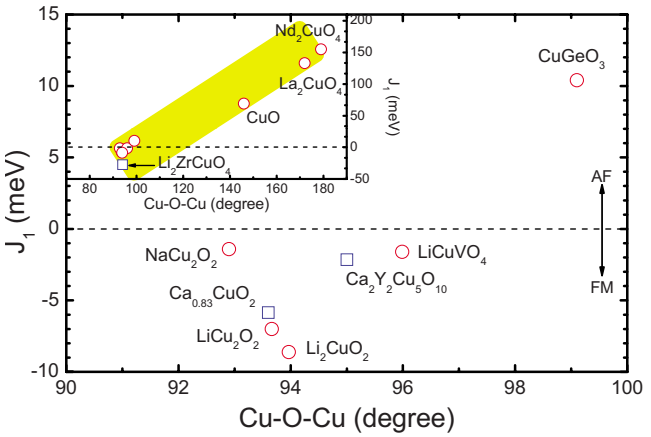

FIG. 2. (Color online) Nearest-neighbor coupling J_1 versus Cu-O-Cu bond angles summarized for some samples with edge-sharing CuO_2 chains, adapted from Refs. 16 and 17. The inset shows values up to 180° for mostly two-dimensional layered structure and the main plot amplifies data near 90° region for the chain compounds. All J_1's are obtained from neutron-scattering experimental studies, except those from susceptibility fitting and labeled as empty square in blue.

the double layer B as shown in Fig. 1(a).[4] Zigzag chain description is only possible when non-negligible coupling J_1^M defined in Fig. 1(b) exists;[4] however, LDA calculations and alternative neutron-scattering spin-wave analysis suggest it to be negligibly small.[8,9] On the other hand, based on the model in Fig. 1(b), the interchain coupling between linear chains through the Cu-O-Cu superexchange $J_\perp$ has been estimated to be comparable to J_2 based on LDA calculations. In particular, Wannier function modified Hubbard model suggests strong orbital overlap between oxygen and the bridged Cu^+ ions, as the J_W defined in Fig. 1(b).[20] These two kinds of structural views led to different assignment of J_1, J_2 and interchain coupling $J_\perp$ but the discrepancy has been resolved based on neutron-scattering spin-wave analysis of alternative fittings.[9] Herein we use the linear chain model with non-negligible interchain coupling in the following description and define J_1, J_2, $\alpha = J_2/J_1$, and interchain coupling $J_\perp$ based on the model shown in Fig. 1(b). When $J_\perp$ is non-negligible as predicted from both calculation and experiment, $J_\perp$ (or J_W) would connect linear chains equally from both sides along the a direction and convert the system from one-dimension to quasi-two-dimension. In fact, such two-dimensional view has been confirmed from its renormalized classical behavior of short-range in-plane magnetic correlation length based on resonant soft x-ray scattering measurement results.[12]

Isotropic spin-1/2 Heisenberg antiferromagnetic chain has been the most widely studied model since the introduction of the Bethe ansatz in 1931.[21] There have been considerable theoretical works on the spin-1/2 chain system with both nearest-neighbor and next-nearest-neighbor of antiferromagnetic interactions as described by the Hamiltonian of

$$H = J_1 \sum (\mathbf{s}_i \cdot \mathbf{s}_{i+1}) + J_2 \sum (\mathbf{s}_i \cdot \mathbf{s}_{i+2}). \quad (1)$$

However, studies on chains with ferromagnetic J_1 and antiferromagnetic J_2 interactions have been rare, and it was only until recently that great interest was refocused on the quantum spin system with emerging electric polarization concomitant of helical spin ordering, such as $LiCu_2O_2$, $LiCuVO_4$, and Li_2ZrCuO_4 as summarized in Fig. 2.[1,4,22,23] Helimagnetic spin ordering for a spin chain occurs when frustrating J_1 and J_2 satisfy a unique condition of $|J_2/J_1| > \frac{1}{4}$ classically. We may also view spin periodicity increases from two (for antiferromagnetic ordering) to infinity (for ferromagnetic ordering) with helical ordering of intermediate commensurate or incommensurate periodicity in between in a classical picture, as described in Fig. 3 by its pitch angle $\theta = \arccos(-J_1/4J_2)$ growing from zero ($J_2/J_1 = -1/4$) to π ($J_2/J_1 = 1/4$). On the other hand, finite chain calculation on one-dimensional quantum spin-1/2 Heisenberg system suggests the occurrence of a gapped twofold spin singlet (dimer) ground state at $J_{nnn}^{AF}/J_{nn}^{AF} = 1/2$ (called Majumdar-Ghosh, MG, point) and a first-order phase transition at $J_2/J_1 = -1/4$ (called FF point) before entering the ferromagnetic regime.[24] The critical ratio of J_2^{AF}/J_1^{AF} to have a gapped phase from the gapless "spin-liquid" ($J_2 = 0$) state for the spin-1/2 antiferromagnetic Heisenberg chain system has been estimated nu-

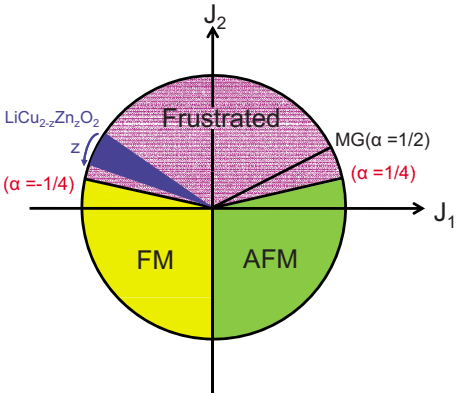

FIG. 3. (Color online) $T=0$ phase diagram of one-dimensional quantum spin-1/2 Heisenberg system with nearest-neighbor J_1 and next-nearest-neighbor J_2 isotropic exchange constants. The Hamiltonian is defined in Eq. (1). Figure 3 is reproduced following Bursill *et al.* (Ref. 24).

merically to be ~0.2411.[25] Finite chain numerical calculations also suggest the occurrence of complex periodicity when approaching the FF point.[24] There are very few quantum spin-chain systems that sit within the second quadrant of the phase diagram shown in Fig. 3, except that the Li_2ZrCuO_4 is claimed to be the one closest to the ferromagnetic critical point,[23,26] $LiCu_2O_2$ of incommensurate helical spin ordering with confirmed ferromagnetic J_1 could be the best candidate so far to explore this region.[22]

Nonmagnetic ion substitution into the low-dimensional quantum spin system has been proved to be not just a simple dilution effect. For example, analytic and quantum Monte Carlo studies on nonmagnetic ion substitution to the Cu site in two-dimensional antiferromagnet La_2CuO_4 is shown to induce substantial frustrating interactions, approximately ≥ 0.4 J per impurity, and can resolve the discrepancy between the experimental and fittings by previous theoretical models.[27] More interestingly, Zn substitution of Cu in the quantum spin chain $CuGeO_3$ induces an unusual antiferromagnetic ordering coexisting with the spin-Peierls (SP) state of spin-lattice dimerization.[28,29] The surprising finding of the coexisting antiferromagnetic and SP states (dimerized antiferromagnetic ordering) is different from the conventional uniform antiferromagnetic state. It is shown that staggered moments can be introduced and with large spatial inhomogeneity in the ordered moment size (correlation length $\xi \sim 10\mathbf{a}$) through spin chain perturbation.[30,31] Clearly nonmagnetic spin zero perturbation is an effective way to probe the mysterious low-dimensional quantum spin system.

We have reported briefly on the finding of an unknown magnetic phase transition in ~10% Zn substituted $LiCu_2O_2$ and its strong correlation to the missing electric polarization previously.[32] Herein, a complete phase diagram mapping is provided in order to explore the impact of nonmagnetic impurity substitution to the quasi-2D spin system in detail. Below ~5.5% Zn substitution, helical ordering temperature $T_h(x)$ reduces as a function of Zn level and follows an interesting finite-size power law, which implies an intriguing domain formation. Novel phase transition below ~20 K is found by ≥5.5% Zn per CuO_2 chain substitution. Magnetic susceptibility measurement results suggest that a new phase transition emerges with a character of spin-gap opening with a magnetic field dependence which is similar to that found in a spin-Peierls phase transition. We tentatively propose one spin dimer model which is consistent to the available magnetic susceptibility, specific heat, and NMR measurement results, a satisfactory model fitting and simulation is given as well. The spin-gap size is found to be roughly proportional to the Zn-substitution level and these isolated dimers are suggested to sit on a background of frustrated spins in the finite spin chains cut short by the Zn defects.

TABLE I. Zn concentrations determined by EPMA and ICP for $LiCu_{2-z}Zn_zO_2$ crystals studied.

Sample ID	z (nominal)	z (EPMA)	z (ICP)
Zn0	0	NA	NA
Zn1	0.01	0.016(3)	0.008(4)
Zn2	0.03	0.034(2)	0.023(7)
Zn3	0.04	0.038(2)	
Zn4	0.045	0.041(1)	
Zn5	0.045	0.052(1)	
Zn6	0.05	0.058(2)	0.050(6)
Zn7	0.10	0.081(3)	0.080(5)
Zn8	0.15	0.109(3)	0.108(4)

II. EXPERIMENTAL DETAILS

A complete series of single crystal $LiCu_{2-z}Zn_zO_2$ with $z \sim 0-0.10$ have been grown using traveling solvent floating-zone (FZ) method. The grown crystals with chemical analysis are summarized in Table I. Feed rod of nominal Zn levels of 0%, 1%, 3%, 4%, 4.5%, 5%, 10%, and 15% are prepared through solid-state reaction route starting from Li_2CO_3: CuO: ZnO mixture of molar ratio $1.2:4-z:z$, where 20% excess Li is added to the initial to compensate for the Li vapor loss. The feed rod is annealed at 750 °C after the thoroughly ground powder mixture is treated at 850 °C under O_2 flow for 12 h each for one time with intermediate grinding. To reduce further Li loss during the molten stage and to prevent Cu^{2+}-rich Li_2CuO_2 impurity phase formation, high-pressure (~0.64 MPa) argon atmosphere is used during crystal pulling and the pulling rate is maintained at 3 mm/hr with 20 rpm feed/seed rods in counter rotation. Li content of the Zn-free crystal has been determined using combined thermal gravimetric analysis (TGA) and iodometric titration methods as reported earlier,[13] and the Cu and Zn contents have been determined using combined inductive coupled plasma (ICP) and electron probe microanalysis (EPMA). While it is impossible to determine the Li content accurately with combined TGA and titration methods for the Zn-substituted samples, and ICP technique alone cannot provide accurate Li content within 10% error, we assume that Li content does not change under the same high pressure Argon atmosphere growth condition and should be maintained near 0.87 ± 0.03 according to our previous conclusions on the

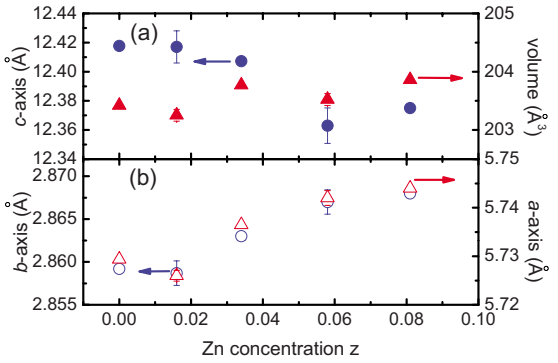

FIG. 4. (Color online) Lattice parameters of $LiCu_{2-z}Zn_zO_2$ with various Zn-substitution levels. (a) The c axis is shown in filled circle and volume is shown in filled triangle, and the circle and triangle in (b) represent b and a axes, respectively.

pure $Li_xCu_2O_2$ crystal.[13] Details of FZ growth and chemical analysis of $Li_xCu_2O_2$ single crystal have been reported previously; however, we describe Li content to be 1 per formula for simplicity in this paper. The homogeneity issue of Zn substitution is examined with EPMA mapping along the growth direction within 2% error within 8 mm and the magnetic phase transition temperature is single and with sharp transition width represented by $d\chi(T)/dT$ peak near phase transition.

Magnetic susceptibilities are measured with superconducting quantum interference device magnetometer (Quantum Design MPMS-XL) with a magnetic field of 1 kOe applied along and perpendicular to the ab plane. The helimagnetic spin ordering cannot be identified clearly from magnetic susceptibilities, where $\chi(T)$ drops smoothly at the transition temperature but can only be identified clearly by its derivative $d\chi/dT$ peaks. Parts of the x-ray structure data were taken using synchrotron x-ray facility NSRRC in Taiwan. For dielectric measurement, the crystals were shaped into a thin disk with thickness approximately 50–100 μm. The top and bottom surfaces were then covered by silver epoxy as electrodes. The dielectric constant was measured by a high-precision capacitance bridge at 1 kHz. At room temperature, the dielectric loss is less than 1,000 nano-Siemens (nS) and decreases at lower temperature reaching 0.02 nS below 30 K. The electrical polarization is determined by integration of the pyroelectric current which is detected at a rate of 0.167 K/s after cooling the samples in a poling field of 1200 kV/m from 50 K. ^{7}Li NMR measurements were carried out based on standard pulsed NMR techniques. Field-swept NMR line shapes were measured by integrating the spin-echo signal at a fixed frequency of $f=33.095$ MHz while sweeping the magnetic field. Spin-lattice relaxation rate $1/T_1$ was measured by applying an inversion pulse prior to the spin-echo sequence with varied delay times.

III. RESULTS AND DISCUSSIONS

Nonmagnetic Zn ion substitution to the spin-1/2 Cu^{2+} site within edge-sharing CuO_2 linear chain is expected to disrupt J_1 effectively and to cut down the infinite chain into even and odd finite chains, although quantum fluctuation, next-nearest-neighbor J_2, and interchain coupling $J_\perp$ could still bring up unexpected results. Although there are two different structural sites of Cu in $LiCu_2O_2$ as shown in Fig. 1, nonmagnetic Zn^{2+} should substitute the Cu^{2+} site only from considerations of both valence and ionic radius. The ionic radius of Zn^{2+} ion (0.74 Å $CN=4$) is similar to that of Cu^{2+} ion (0.71 Å $CN=4$) for square planar coordination within the CuO_2 chain, which is significantly larger than that of a Cu^+ ion (0.60 Å $CN=2$) within the CuO_2 dumbbell.[33] Room-temperature lattice parameters for $LiCu_{2-z}Zn_zO_2$ as a function of Zn-substitution level is summarized in Fig. 4. We note a significant reduction of c axis in concomitant with slight increase of a and b axes when crossing the $Zn\sim5\%$ boundary with minimal change on the cell volume. These results suggest the success of Zn substitution to the Cu^{2+} instead of the smaller Cu^+ site within the bridging O-Cu-O dumbbell and the average lattice distortion must be intimately correlated with the occurrence of novel phase transitions found for $z>0.05$ at low temperature to be discussed further in the text.

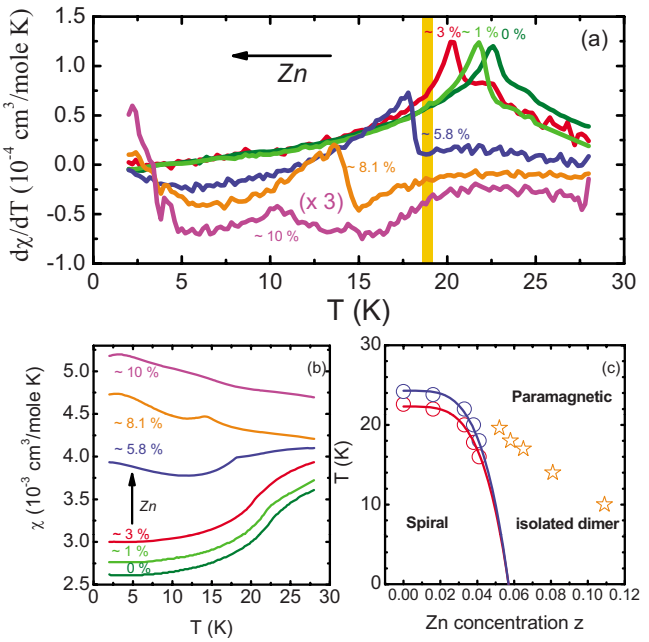

FIG. 5. (Color online) Temperature dependence of $d\chi_{ab}/dT$ for $LiCu_{2-z}Zn_zO_2$ along the ab plane with $z=0\%$, 1.6%, 3.4%, 5.8%, 8.1%, and 10.9%. For clarity, the signal for $z=10.9\%$ is multiplied by three. $\chi(T)_{ab}$ data are shown in (b), which are normalized to the $\chi(300\ \mathrm{K})$ value of the 0% sample. The helical ordering temperature T_h versus Zn content is summarized in (c). Finite size scaling behavior is found for Zn below ~5.5% for the two transition temperatures with H applied along the ab plane and c direction.

A. Magnetic susceptibilities

Figure 5 summarizes the complete evolution of Zn-substitution effect shown in $\chi_{ab}(T)$ and $d\chi_{ab}/dT(T)$ data for all samples studied. Low Zn substitution reveals typical signature of anisotropic helimagnetic ordering transition and reduces T_h slightly below $Zn\sim5.5\%$ per CuO_2 chain to show peaks of $d\chi(T)/dT$ at ~20 and 22.5 K, which are slightly

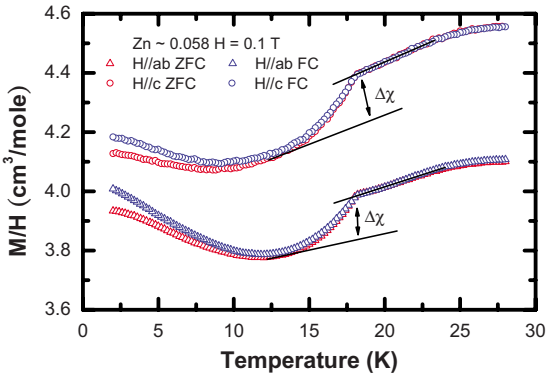

FIG. 6. (Color online) Magnetic susceptibilities for Zn~5.8% sample with field applied along the *ab* and *c* directions. An estimate of susceptibility reduction is obtained from $\triangle\chi/\chi$ at T_c.

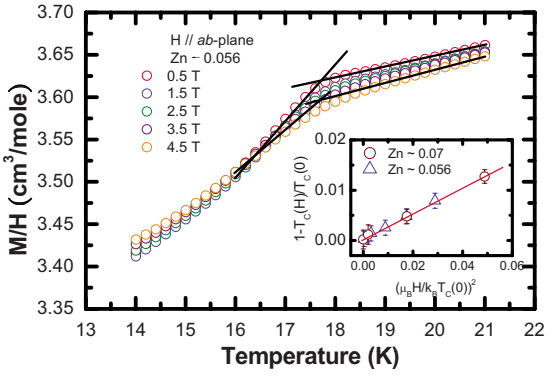

FIG. 7. (Color online) Magnetic susceptibilities of single crystalline $LiCu_{2-z}Zn_zO_2$ measured near the phase transition temperature $T_c(H)$ in the range of H=0.01–4.5 T. $T_c(H)$ value is defined by the intersection of two linear fitted lines from above and below. A universal plot of $1\text{-}T_c(H)/T_c(0)$ versus $[-\mu_B H/k_B T_c(0)]^2$, including two samples of different Zn levels above ~5.5%, is shown in the inset with a linear fitting of slope ~0.26.

lower than that of the pristine crystal but similar to the nearly Li deficiency-free sample as reported previously.[3,13] Across the Zn~5.5% phase boundary, $\chi(T)$ transforms from a spiral spin ordering character toward a steplike crossover or a cusp shape near the phase transition as shown in Fig. 5(b). The different characters for the helical and the novel phase transition are displayed not only by the symmetry change of $d\chi(T)/dT$ peak shape but also by its smooth crossover ($\leq$5.5%) versus cusp shape ($\geq$5.5%) difference in $\chi(T)$.

The lowering T_h for helical spin ordering with Zn $\leq$5.5% per CuO_2 chain suggests that the helical spin ordering condition of $|J_2/J_1| > \frac{1}{4}$ must be met still, which is not surprising considering the perturbed spin chains through low level nonmagnetic ion substitution. Low Zn substitution does not break the original spiral spin ordering but only reduces its transition temperature slightly from ~22 K to the lowest ~20 K before two coexisting phases emerge. It is interesting to note that the single phase sample of the lowest T_h has been achieved through $Li_{0.99}Cu_2O_2$ before, and similar ~20 K transition temperature is found when the Li deficiency is reduced to the minimum.[13] Clearly the spiral spin ordering of $LiCu_2O_2$ system prefers an optimum level of Cu^{2+} excess (~0.17/f.u.) instead of exactly equal amount of Cu^+ and Cu^{2+}, which must be strongly correlated with the required incommensurate periodicity of spiral spin ordering with modulation ζ=0.174 along the chain **b** direction while the periodicity is intimately related to the J_2/J_1 ration classically.[12] Current phenomenon of T_h reduction as a result of Zn substitution could be due to the finite chain effect, i.e., the Zn substitution cuts off the original helically ordered infinite chains before the optimal incommensurate modulation for the spiral ordering is broken. While J_1 may be frustrated locally near the Zn site, the average J_2/J_1 ratio may not be modified very much at Zn levels lower than ~5.5%, which in fact has been supported from our high-temperature series expansion (HTSE) fitting results to be discussed below.

The Zn substitution above ~5.5% per CuO_2 chain introduces an intriguing phase transition which is hard to identify based on its $\chi(T)$ character of nearly isotropic cusp shape as shown in Fig. 6. Since the newly discovered phase transition is nearly isotropic for this quasi-two-dimensional system of specific spiral plane, it is unlikely that the transition to be antiferromagnetic ordering or even spin glass. The steplike isotropic reduction of spin susceptibility implies the existence of a gapped phase that comes from part of the system, judging from its nonzero susceptibility at low temperature, even after a background subtraction of expected enhancing Curie contribution from Zn-introduced isolated spins. As shown in Fig. 6, the ratio of χ step reduction versus peak χ value at T_h ($\triangle\chi/\chi$ at T_c) is very close to the Zn-substitution level between ~0.045–0.055, which implies that only part of the system falls to the gapped ground state and is proportional to the Zn level, i.e., high Zn substitution introduces a gapped phase that is proximate to the Zn centers. On the other hand, more pronounced hysteresis is observed in particular below 5 K, which implies that glassy or irreversible domain effect occurs below T_c. Bobroff *et al.*[34] have proposed that Zn impurities could introduce collective spin freezing around each impurity center for spin gapped system at low temperature, which may also apply to the gapped phase in our system as suggested by the spin glasslike behavior below ~5 K. Further muon spin-resonance experiment is planned to examine this proposed explanation.

We traced magnetic field dependence of transition temperature of crystals with Zn level higher than ~5.5% and found the scaling of $1\text{-}T_c(H)/T_c(0)$ shows a convincing H^2 dependence as seen in the inset of Fig. 7. The transition temperatures have been determined by linear extrapolation from the upper and lower parts of the susceptibility data near T_c before they deviate again due to Curie contribution, similar to that found in the Zn-substituted spin Peierls compound $CuGeO_3$.[35] Bulaevskii *et al.*[36] have shown that commensurability effect in SP transition would cause strong magnetic field dependence of T_c in the limit of $\mu_B H \ll k_B T_c(0)$ to follow as equation

$$1 - \frac{T_c(H)}{T_c(0)} \sim \beta \left[\frac{\mu_B H}{k_B T_c(0)} \right]^2. \quad (2)$$

Such field dependence is a result of band filling change that is sensitive to the competing commensurability-incommensurability requirement between spin and phonon

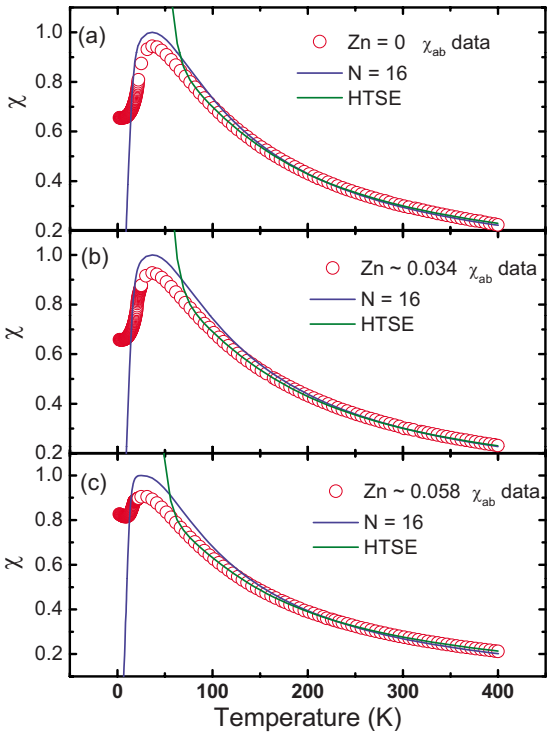

FIG. 8. (Color online) HTSE fitting and exact Hamiltonian diagonalization using 16 spin ring simulation results of magnetic susceptibility data for samples with Zn ~ 0%, 3.4%, and 5.8%.

for spin-Peierls transition. We find that there is clear H^2 dependence for the reduced critical temperature. Such H^2 field dependence has been observed in $CuGeO_3$ of well-known SP transition before.[35] The quadratic field dependence found in Eq. (2) also ruled out the possibility of ordinary structural transition due to phonon instability under strong field.[36] There is no evidence of structural transformation or signature of lattice doubling found based on our synchrotron x-ray structure analysis for the whole Zn-substituted series (not shown). The proportional constant β shown in Eq. (2) is fitted to be ~0.26, which is lower than the 0.46 found in the dimerized system $CuGeO_3$ but higher than the calculated value of 0.11 within Hartree-Fock approximation.[35,36] Moreover, we find such quadratic field dependence of T_c is independent of Zn content as shown in Fig. 7, which implies that the same universality class applies to the impact of Zn substitution above ~5.5%; and this implication must be clarified further in the future both experimentally and theoretically.

B. Finite-size scaling

Figure 5 shows that helical ordering transition temperature $T_h(z)$ for $LiCu_{2-z}Zn_zO_2$ decreases with higher z before it drops precipitously for $z \sim 0.055$ critically. The precipitous drop of $T_h(z)$ suggests a power-law z dependence of large exponent. Fitting $T_h(z)$ with reduced temperature and z in power law as

$$1 - \frac{T_h(z)}{T_h(0)} = \left(\frac{z}{z_c}\right)^n \propto L^{-1/\nu} \tag{3}$$

and we find the exponent n to be near 4 as $T_h(0)$, z_c and n are left as free parameters in the fitting. An equally good fitting

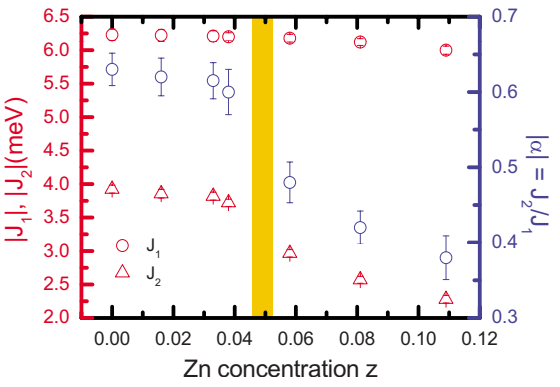

FIG. 9. (Color online) J_1, α, and J_2 (converted from α) obtained from HTSE fitting results versus Zn-substitution level for $LiCu_{2-z}Zn_zO_2$.

is obtained when n is fixed at 4, and $T_h(0)$ and z_c return to be 22.3(3) (for $H \| ab$), 24.3(3) (for $H \| c$) and 0.057(2), respectively. The satisfactory fitting of Eq. (3) suggests that finite size effect is able to describe the z dependence of T_h. Finite-size scaling has been applied in Monte Carlo simulation using limited size L and its size extrapolated exponent ν to calculate the critical temperature in real infinite size matrix as described in Eq. (3).[37] Since the critical exponent ν within mean field approximation to be 1/2, the fitted $n=4$ suggests that T_h reduction is a result of limited correlation length due to finite size, i.e., $L(z) \propto 1/z^2$. The most natural model that can explain such z dependence of $L(z)$ would be a picture of two-dimensional helical ordered domains which are cut off by defect or secondary phases formed domain boundaries, the higher the Zn level the smaller the domain size $\sim \mathbf{a}(\mathbf{b})/z^2$. Assuming dopants are distributed at the two-dimensional domain boundaries, the effect of lower T_h can be explained as a result of cut-off correlation length by the domain boundaries. Since the in-plane magnetic correlation length ξ_{ab} for the pure $LiCu_2O_2$ has been estimated to be ~1200 Å,[12] which is very close to the domain size estimated for $z \sim 0.055$ at the phase boundary, i.e., $L = b/0.055^2 - 1000$ Å. It is implied that long range helimagnetic spin ordering is destroyed totally once the domain size becomes smaller than the helical magnetic correlation length.

The original undoped sample has a quasi-two-dimensional matrix of helical ordered incommensurate spin structure with periodicity about 5.7**b**, i.e., modulation vector $\zeta \sim 0.174$ along the **b** axis with pitch angle 62.6°.[12] We find that the phase boundary for Zn ~ 5.5% is very close to the onset of nonzero probability of aggregated (more than one) Zn per $6\mathbf{b} \times 2\mathbf{a}$ magnetic supercell of incommensurate helical ordering, i.e., starting from 2 out of ~35 Cu sites are substituted by Zn. The estimated phase boundary agrees very well with the phase boundary z_c obtained from the finite-size scaling fitting as discussed previously. The phase boundary obtained from simple probability analysis suggests that long-range helical ordering is suppressed only when more than one Zn exist per unit superlattice of incommensurate helical ordering. For Zn-substituted sample prepared from high temperature melt, it is reasonable to assume that Zn ions distribute randomly. Although it is unreasonable to assume Zn to be mobile at low temperatures, we suspect that the comparable

TABLE II. Exchange coupling constants J_1 and $\alpha=J_2/J_1$ obtained from HTSE method and exact diagonalization of the Hamiltonian with 16 spin ring ($N=16$) simulation. Estimations from neutron-scattering spin-wave analysis and LDA calculation are listed for comparison.

	HTSE			Neutron study (Ref. 9)			LDA (Ref. 8)		
Zn content (EPMA)	J_1 (meV)	α	$N=16$ α	J_1 (meV)	α	$J_\perp$	J_1 (meV)	α	$J_\perp$
0	−6.23(1)	−0.63(2)	−0.578	−5.95[a]	−0.62 [a]	0.9[a]	−8	−1.777	5.7
				−7[b]	−0.535[b]	3.4[b]			
0.016(3)	−6.22(2)	−0.62(1)							
0.034(2)	−6.21(3)	−0.61(1)	−0.54						
0.038(2)	−6.20(2)	−0.60(3)							
0.058(2)	−6.18(2)	−0.48(4)	−0.468						
0.081(3)	−6.12(3)	−0.42(2)							
0.109(3)	−6.00(1)	−0.38(1)							

[a]Model 1 of Ref. 9.
[b]Model 3 of Ref. 9.

and competing (frustrating) couplings J_1, J_2, and $J_\perp$ could transport spin degree of freedom from Zn centers to the domain boundaries that surround helically ordered spins. Such phenomenon could be viewed as a microscopic phase separation with localized spins confined within domain boundaries and encircle domains with spins of persisted helical ordering, an interesting contrast to the phase separation resulting from one-dimensional charge stripe separated antiferromagnetic domains in $La_{2-x}Sr_xCuO_4$.[38]

C. HTSE and exact diagonalization fittings

In order to trace the frustrating couplings J_1 and J_2 ($\alpha=J_2/J_1$) for this helimagnetic system, we applied HTSE and exact Hamiltonian diagonalization methods to fit the magnetic susceptibility data for the entire Zn-substitution range. Starting from Hamiltonian written as Eq. (1), the HTSE uses expansion coefficients for the frustrated quantum spin-chain model calculated by Bühler *et al.*[39] Exact diagonalization of the Hamiltonian using 16 spin ring ($N=16$) calculation is used to provide satisfactory temperature dependent fitting at high-temperature range after peak normalization and background subtraction. Both HTSE and $N=16$ fittings return satisfactory results on high-temperature range and agree very well on the estimation of J_1 and α as shown in Fig. 8 and summarized in Fig. 9 and Table II. These results are in agreement with those obtained from LDA calculation and neutron scattering spin wave analysis.[8,9] The fitting results using $N=16$ finite chain are in agreement at high-temperature range with HTSE within 6(1) %, although the low temperature region deviates significantly as a result of gapped finite-size chain approximation. We find J_1 decreases smoothly, crossing the ~5% Zn phase boundary by ~4% only while J_2 (calculated from J_1 and α) reduction is far more pronounced. The significant J_2 reduction through Zn substitution moves this frustrated system closer to the quantum critical point near $\alpha=-1/4$ as shown in Fig. 3 and complex periodicity may have occurred.[24,26]

While high Zn substitution is proposed to introduce isolated dimers into the original long-range helical spin ordered system, the magnetic susceptibility measurement results should reflect such assumption, i.e., the final form of $\chi(T)$ for Zn $\geq 5.5\%$ must include contributions from a gapped state of isolated dimers as well as the isolated spins that shows paramagnetic behavior. We fit the high Zn data additionally with combined HTSE, isolated dimer, and Curie contributions as shown in Fig. 10, following equation:

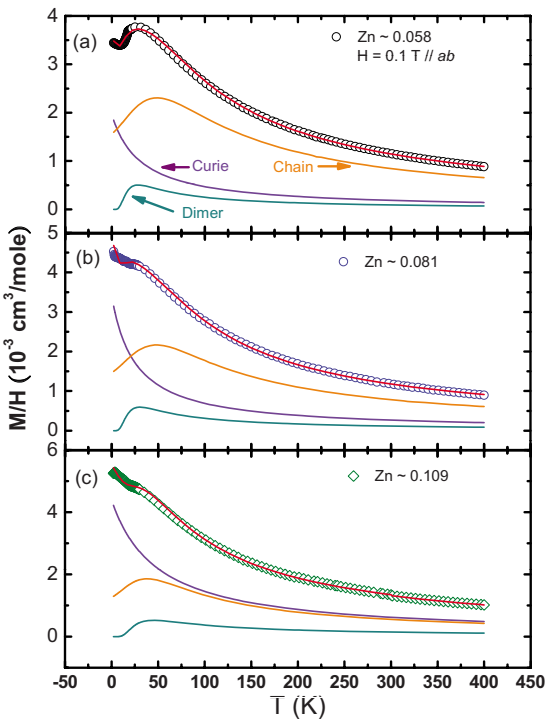

FIG. 10. (Color online) Combined HTSE, isolated dimer and Curie-Weiss model fitting.

TABLE III. Magnetic susceptibility fitting results of high Zn-doping level by the proposed model of combined spin chain, isolated dimers, and spins following Eq. (4).

	z=0.06(1)	z=0.08(1)	z=0.11(1)
N_{chain}	0.82	0.76	0.52
J_c (K)	37.5(2)	37.0(3)	29.5(5)
N_{CW}	0.1	0.14	0.35
Θ (K)	−31.6(9)	−25.6(4)	−49.4(7)
C	0.62(6)	0.62(4)	0.60(2)
N_D	0.08	0.10	0.13
J_D (K)	45.8(6)	48.7(5)	91.8(3)
$\Delta\chi/\chi(T_c)$ (%)	4.5(1)	7(1)	0.5(3)

$$\chi = \chi_0 + N_{chain}\chi_{chain} + N_D\chi_{Dimer} + N_{CW}\chi_{CW},$$

$$= \chi_0 + N_{chain}\frac{1}{T}\sum_{n,k} a_{n,k}\alpha^k\left(\frac{J_1}{k_BT}\right)^n + N_D\frac{N_Ag^2\mu_B^2}{k_BT(3+e^{J_D/k_BT})}$$

$$+ N_{CW}\frac{C}{T-\Theta}. \quad (4)$$

The only constraint used in the fitting process is the normalization of $N_{chain}+N_{dimer}+N_{Curie}=1$. The complete fitted results are summarized in Table III. Temperature dependence of isolated dimers with spin gap size J_D follows the Bleany-Bowers equation, which can be reduced to describe the low-temperature spin-gap behavior and the Curie-Weiss behavior for dimers at high temperature.[40] The fitted results using Eq. (4) are not perfect, possibly due to the incomplete HTSE chain description, neglected interchain coupling, and the possible short-range coupling among dimers; however, it does provide a better fitting below T_c for higher Zn above ~5.5%. The amount of dimer phase N_D is nearly proportional to the Zn content level, which supports a picture of Zn-introduced isolated dimers favorably. Moreover, the fitted values of J_D agree very well with the LDA and neutron-scattering estimation of $J_\perp$ (see Table II), which supports a scenario of dimer formation as a result of O-Cu^+-O bridged nontrivial interchain coupling $J_\perp$. The Curie contribution from isolated spins, N_{CW}, increases drastically for $z\sim0.11$, which is reflected on the weaker and broadened phase transition as shown in Fig. 5(a) also. Following the same phase separation model suggested here, we find that the magnetic susceptibility reduction at $T_c[\Delta\chi/\chi(T_c)]$ also reflects the spin-gapped phase proportion as summarized in Table III, before it is smeared by the significantly enhanced Curie contribution at $z\sim0.11$. Both the $\chi(T)$ model fitting and the susceptibility reduction at T_c have demonstrated satisfactory agreement on the fraction of isolated dimer phase and the Zn content for $z\geq5.5\%$, which supports the interpretation of the special magnetic susceptibility anomalies near T_c (see Fig. 5) based on a scenario of phase separation.

D. NMR

To gain further insight on the nature of the anomaly observed in the temperature dependence of χ for heavily Zn-doped crystals, we also carried out NMR measurements for ^{7}Li (nuclear spin $I=3/2$, nuclear gyromagnetic ratio $^7\gamma_n/2\pi=16.546$ MHz/T) in $LiCu_{2-z}Zn_zO_2$ ($z\sim0.058$) by applying an external magnetic field B along the crystal c axis. We chose the NMR carrier frequency $f=33.095$ MHz so that we could compare our NMR results for Zn-doped sample with an earlier NMR report for undoped $LiCu_2O_2$ by Gippius *et al.*[8] At 100 K, we observe a typical NMR line shape expected for nuclei with spin $I=3/2$ with three distinct peaks split by the c-axis component of the nuclear quadrupole interaction, ν_Q^c. As shown in Fig. 11, the central peak near $B=2$ T arises from the nuclear spin $I_z=+1/2$ to $-1/2$ transition while two additional peaks near $B=1.997$ T and 2.003 are from the $I_z=\pm3/2$ to $\pm1/2$ transitions. From the splitting, 0.0030 T, between the peaks, we estimate $\nu_Q^c = {}^7\gamma_n\cdot0.0030=0.05$ MHz.

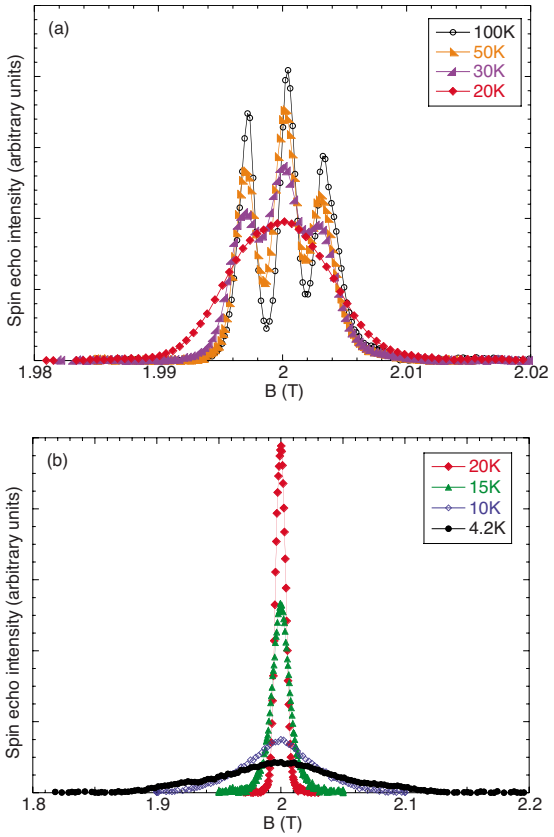

FIG. 11. (Color online) Representative results of field-swept ^{7}Li NMR line shapes measured at $f=33.095$ MHz, (a) at 20 K or above, and (b) at 20 K or below. The external magnetic field was applied along the crystal c axis. Notice that the scales of horizontal axis are different by a factor of ten between the two panels.

Upon further cooling, all three peaks progressively become broader. In principle, there are two possible mechanisms of the NMR line broadening in a paramagnetic material, i.e., magnetic effects or quadrupolar effects. In the first scenario, all three peaks should broaden by an equal amount while only the satellite peaks broaden in the second scenario. The observed line shapes at 50 and 30 K clearly show that all three peaks are equally broadened hence we conclude that there exists slight magnetic inhomogeneity. This is consistent with the fact that Zn^{2+} ions substituted Cu^{2+} sites to remove

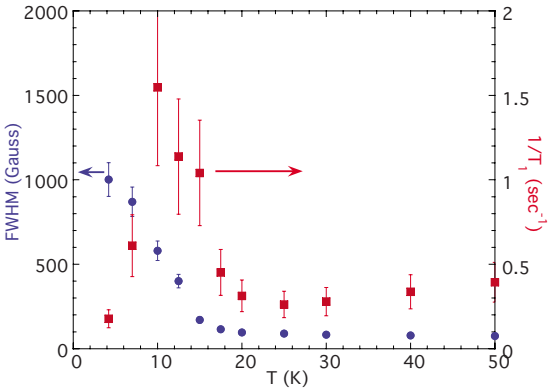

FIG. 12. (Color online) The temperature dependence of (a) the FWHM of the ^{7}Li NMR line shape and (b) the nuclear spin-lattice relaxation rate $1/T_1$ measured at the center of the line shape.

the electron spin $S=1/2$, thus introducing random disorder in the matrix of $S=1/2$. The splitting ν_Q^c between the peaks remains unchanged within experimental uncertainties down at least to 30 K. This implies that electric field gradient at the ^{7}Li site does not change significantly in this temperature range. Below 20 K, the line broadening becomes so severe that we can no longer observe the quadrupole splitting between the three peaks. At 10 and 4.2 K, we observe an extremely broad line shape with a very broad peak centered around 2 T and two equally spaced shoulders near 1.92 and 2.08 T. We summarize the temperature dependence of the full width at half maximum (FWHM) of the NMR line shape in Fig. 12. The FWHM begins to increase dramatically below ~18 K, where χ in Fig. 6 shows a well-defined kink.

It is very instructive to compare these NMR line shapes with those observed for undoped $LiCu_2O_2$ by Gippius *et al.*[8] under nearly identical experimental conditions. Our results above 30 K are very similar to the undoped case but our lineshape at 4.2 K is strikingly different from that observed for $LiCu_2O_2$. In the latter case, Gippius *et al.* demonstrated that two large "horns" develop at 1.95 and 2.05 T, accompanied by two additional horns near 1.9 and 2.1 T (see the upper panel of Fig. 3 by Gippius *et al.*). They also demonstrated that these four horns are the consequence of the distribution of hyperfine magnetic fields at ^{7}Li sites, arising from an incommensurate spiral modulation of magnetic moments. Our NMR line shape at 4.2 K does not exhibit such sharp horn structures but the overall shapes do bear a strong resemblance to each other. The smearing of the sharp horns in our case is naturally understood as the consequence of disorder induced by Zn ions in the incommensurate modulation of magnetic moments.

The establishment of this low-temperature-modulated state with strong disorder is unlikely to be due to a second-order phase transition. In the case of a conventional second-order magnetic phase transition, the nuclear spin-lattice relaxation rate $1/T_1$ would diverge at the phase transition temperature because of the critical slowing down of the magnetic moments. In contrast, $1/T_1$ measured at the center of the ^{7}Li NMR line shape does not diverge near 18 K in the present case. Instead, we observe a broad hump centered around 12 K. This is consistent with glassy development of

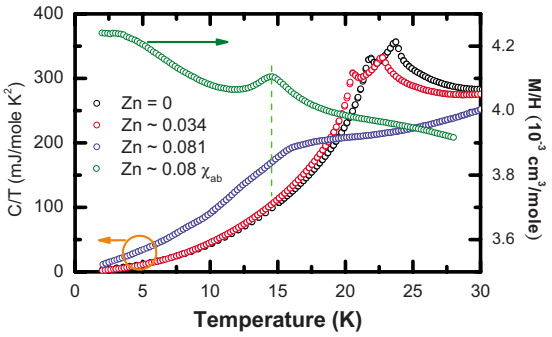

FIG. 13. (Color online) Specific heat of $LiCu_{2-z}Zn_zO_2$ with Zn=0, 0.034, and 0.081. χ_{ab} for Zn=0.081 is displayed also to show T_c defined by the cusp shape anomaly.

the modulated ground state. Such glassy behavior has also been demonstrated by the pronounced thermal hysteresis in the magnetic susceptibility measurement shown in Fig. 6. It is reasonable to assume that the NMR results describe properties of the major spin population in the system, besides the isolated dimers or spins suggested above. The glassy development below ~12 K could be coming from the frozen short-range ordered spins within the frustrated finite spin chains.

E. Specific heat

Specific heats for samples with different levels of Zn substitution are shown in Fig. 13. The undoped and low Zn ($\leq$5.5%) samples show typical double peaks which correspond to the two distinct transition temperatures along the **ab** and **c** directions, respectively, for the spiral spin ordering. Low Zn sample of 3% substitution does not alter the transition width and simply shift the transition doublet to slightly lower, which indicates the robust nature of the helical spin ordering on zero spin perturbation. On the other hand, a significantly broader specific-heat anomaly is observed near ~14 K for Zn~8% sample, in fact there are two very broad peaks sitting above and below T_c as defined by the cusp of $\chi(T)$. These broad anomalies suggest that either the phase transition is of short range in nature, or significant inhomogeneity exists in this Zn substituted crystal. The existence of broad C_p peaks together with the clear $\chi(T)$ cusp observed at T_c suggests that short-range ordering of spin glasslike behavior occurs. Although it is tempting to interpret the coexisting broad C_p anomaly and $\chi(T_c)$ cusp to be coming from a well-defined spin-glass phase transition, we cannot ignore the fact that there are two broad peaks of C_p across T_c, besides, the thermal hysteresis of $\chi(T)$ is not pronounce enough immediately below T_c and only developed at much lower temperature as suggested by both the $1/T_1$ and $\chi(T)$ below ~5–10 K. A reasonable interpretation can be obtained following our proposed phase separation scenario, i.e., we might view the broad "doublet" to be coming from short-range ordering of the frustrated spins (of reduced J_2/J_1 ratio) on the finite spin chain, which has been cut short by the Zn ions, while the cusp at $\chi(T_c)$ is a result of spin-gap opening from those isolated spin dimers.

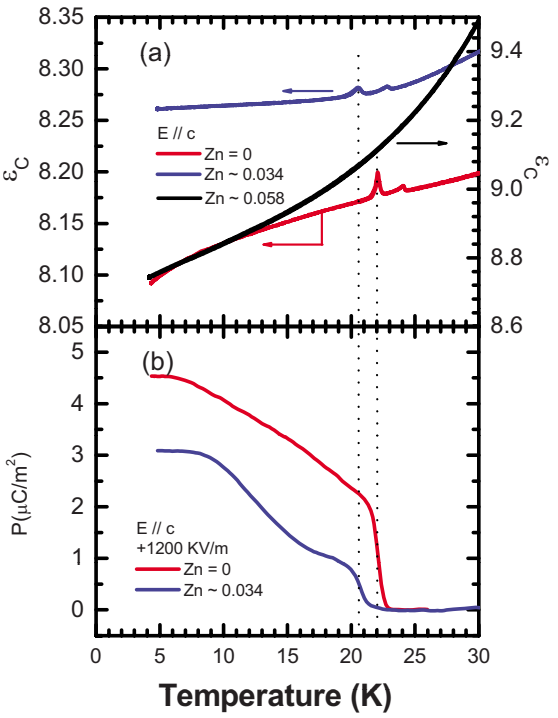

FIG. 14. (Color online) Electric polarization and dielectric response along the *c*-direction for $LiCu_{2-z}Zn_zO_2$ with Zn=0, 0.034, and 0.058. An electric field of 1200 kV/m has been applied above the transition temperature before each measurement.

Magnetic entropy ΔS_M can be extrapolated from C_p after the subtraction of lattice contribution and integrating from 2 to 160 K. The entropy difference between the pure and the ~8% Zn-substituted samples is estimated to be 580 mJ/mole K, which is rather close to a portion (z) of the total Cu^{2+} spins in the system as $zR\times\ln(2S+1)=0.081\times8.3\times\ln 2=470$ mJ/mol K, i.e., due to the missing spins for gapped singlet formation as a result of Zn substitution. It is also of interest to extract the magnetic entropy ΔS_M from C_p. For this purpose, C_p of $LiCu_2O_2$ between 160 and 300 K (data not shown) was fit by the Debye model with only one parameter, i.e., the Debye temperature Θ. The fitting-temperature range was chosen so as to avoid the contribution of the orderings at low temperatures. The one-parameter Debye model gives a nearly perfect description of C_p within this temperature range, and leads to $=574\pm3$ K for $LiCu_2O_2$. With the lattice contribution resultant from the fit, ΔS_M can be extract from C_p after the subtraction of lattice contribution and integrating from 2 to 160 K. A significant portion of ΔS_M is found above T_C. This result is qualitatively similar to that reported in Ref. 4, however with a quantitative difference. Generally, there could exist some uncertainties in the determination of the lattice contribution of C_p proximate to the temperature regime of T_C. It is quite puzzling to note that the integrated $\Delta S_M\sim18$ J/mole K is almost three times larger than the theoretical expectation, i.e., $\Delta S_M=R\ln 2=5.8$ J/mole K for an $S=\frac{1}{2}$ system. This discrepancy must be due to certain factors other than phonon or spin. A possible candidate could be the long- or short-range ferroelectric ordering. Details of the specific-heat study will be reported elsewhere.

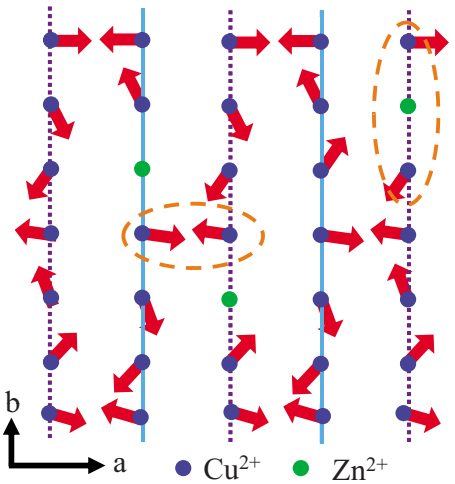

FIG. 15. (Color online) A proposed dimer configuration for high Zn-substituted (≥5.5%) sample below the phase transition temperature. This figure is constructed by randomly distributing Zn on a two-dimensional spiral ordered background with a incommensurate $2\mathbf{a}\times6\mathbf{b}$ magnetic superlattice (modulation $\zeta=0.174$) periodicity along the **b** axis. The alternating dot purple and solid blue colored lines are not in the same plane but bridged by Cu^+ as a quasi-two-dimensional bilayer A as shown in Fig. 1.

F. Electric polarization

Dielectric constant and electric polarization have been measured for $LiCu_{2-z}Zn_zO_2$ ($z\sim0,0.034,0.058$) single crystals along the *c* direction and shown in Fig. 14. The undoped sample shows the onset of electric polarization below ~22 K and two anomalies near 22 and 24 K in dielectric constant similar to those reported in the literature.[3] 3.4% Zn substitution reduces the spiral ordering temperature and electric polarization slightly. 5.8% Zn-substitution sample shows no trace amount of electric polarization near its magnetic transition temperature near 14 K as indicated in Fig. 5. Spin-current or inverse Dzyaloshinskii-Moriya mechanism has been applied to interpret the origin of electric polarization through spiral spin ordering and has been tested by chirality reversion experiment.[2,3] Current dielectric constant measurement results once again confirm that long-range spiral spin ordering is a prerequisite for the spontaneous electric polarization in current system.

G. Proposed dimer models

For a system composed of coexisting isolated spin dimers on a short-range ordering helical background, Fig. 15 shows two simplified dimer models we proposed to describe the observed gapped experimental results for Zn-substitution level higher than 5.5%. In the first possible scenario, singlet dimers could form due to non-negligible antiferromagnetic interchain coupling $J_\perp$ (or J_W, see Fig. 1) for interchain coupled spins near Zn pairs. Effective antiferromagnetic interaction between spins near Zn impurity located on different chains can also be nonzero for coupled frustrated quantum spin chains, where four-spin coupling (cyclic exchange) has been considered.[41,42] Since the ferromagnetic J_1 is disrupted locally by Zn impurity and the antiferromagnetic J_2 becomes

dominant locally, the second possible scenario can be described by dimers formed with antiferromagnetic coupled Cu^{2+} ions (J_2) across the Zn impurities within the same chain (see Fig. 15). Such gapped excitation described by a confined spin 1/2 soliton has various gap sizes as spin chain is cut short from the gapless infinite system to various finite lengths.[43] The distribution of gapped excitations can also be reflected on the nonvanishing spin gap, broad C_p peaks and ^{7}Li NMR $1/T_1$. Isolated spin dimers or aggregated clusters coexist on the short-range ordered finite spin chain background when Zn level is above ~5.5% below T_c. The proximity of T_c defined by $\chi(T)$ reduction onset and the broad short-range ordering signature in $C_p(T)$, as described in Fig. 13, suggest that the coupling strength of short-range ordering background spins is comparable or even prerequisite to the isolated spin dimerization near Zn pairs.

For Zn level below ~5.5%, dilute isolated spins introduced by Zn should distribute randomly near doped Zn centers. However, the observed finite-size scaling behavior discussed above seems to suggest a scenario that these isolated spins could "transport" to the domain boundaries encircled the long-range helical ordering spins, while Zn impurity should not be mobile at such low temperatures. Potential spin-transport mechanism could be described as a soliton, which can be formed near Zn center and transport through the frustrating helical ordered spin background. Such behavior supports a picture of finite size effect for Zn $\leq$ 5.5% and the short-range ordered dimer cluster formation for Zn higher than 5.5%, both of which require spin transport assisted phase separation on the frustrating background. Mechanism for creation and propagation of a chiral soliton pair on a spiral ordered spin-chain background has been described theoretically.[43] While nonmagnetic Zn ions break the original infinite spin chain of helical spin ordering, soliton pair formed around Zn centers could be transported through this intrachain gapless excitation mechanism until it hit the next Zn impurity, which could be a starting point on interpreting our findings in this study and a detailed calculation is necessary.

Peierls transition has been one of the most common electronic instability mechanisms for the one-dimensional system. There are two types of spin dimer formation, with or without spin-phonon interaction, i.e., whether there is phonon assisted local structure distortion as singlet dimer forms. Since the phonon assisted spin-Peierls transition requires translational symmetry breaking, i.e., the lattice doubling which loses translational symmetry to open a gap near the Fermi level, which is a collective phenomenon for the one-dimensional spin system. Although the magnetic field dependence of T_h shown in Fig. 7 suggests that the gapped phase has a spin Peierls system character, we have not found evidence of lattice doubling from synchrotron x-ray diffraction results so far. In fact, it is not expected to be observed based on phase separation model, i.e., the phase fraction of isolated dimers is proportional to the Zn level of $\leq$10% only. On the other hand, we find that J_2 and $J_\perp$ are both antiferromagnetic and of comparable strength according to LDA calculation and neutron-scattering spin-wave analysis.[8,9] Spins near Zn pair centers must face the frustrating interaction between antiferromagnetic J_2 and $J_\perp$. Interestingly, several LDA and spin-wave analysis models suggest the ratio of antiferromagnetic $J_\perp/J_2$ to be near 1/2, another condition that satisfies the Majumdar-Ghosh dimerization without phonon-assisted lattice distortion.[44] Whether the dimerization occurs with or without phonon interaction, a local probe on subtle structure distortion is necessary; however, it would be difficult to verify if only a fraction ($\sim z$) of the spins to demonstrate spin dimerization.

Microscopic phase separation due to extrinsic inhomogeneity can often been observed in samples prepared in powder form or thin film on a substrate. On the other hand, phase separation of electronic origin could be an intrinsic property in a strongly correlated material system and has attracted studies from many aspects, particularly for superconductor and colossal magnetoresistance materials.[45–47] Since current finite-size effect and spin-dimer glass behavior are observed in single-crystal sample with randomly distributed zero spin ions on a quantum frustrating helimagnetic background, the phase separation phenomenon in Zn-substituted $LiCu_2O_2$ system must be of electronic origin. In particular, even though the driving force remains to be explored theoretically, separated phases distinguished by different spin order/disorder types are unique and have never been reported before.

It is interesting to note that the phase diagram summarized in Fig. 5 shows high similarity to phase boundary and Zn dependence for the general phase diagram as summarized by Bobroff *et al.*[34] on Zn-substituted spin-gapped systems. For the gapped systems including isolated ladders, Haldane or spin-Peierls chains, Zn impurities are proposed to induce extended magnetic moments that freeze at low temperatures. Zn impurities must introduce similar residue spins as shown in Fig. 15 on the spiral ordered background, which could explain the spin freezing phenomenon observed near ~5 K from NMR and magnetic susceptibility measurement results discussed above.

The existence of singlet spin dimer has been predicted from density matrix renormalization group type algorithm calculation by Furukawa *et al.* for one-dimensional quantum frustrated spin chain with a Hamiltonian similar to Eq. (1), where nontrivial easy plane exchange anisotropy is considered also in order to simulate the asymmetric ^{7}Li NMR spectra accurately.[8,48] We note that the high Zn-substituted samples with J_2/J_1 ratios summarized in Table II could fall in the range of dimerization according to the phase diagram constructed by easy-plane anisotropy vs J_1/J_2 as proposed by Furukawa *et al.* In particular, the J_2/J_1 ratio drops significantly as system crosses over the ~5.5% Zn boundary from the original chiral spin ordering to the partially gapped spin dimerization state. However, we must point out that the phase diagram proposed by Furukawa *et al.* is based on an infinite chain system calculation while current Zn substituted spin chains are finite of unequal lengths, which could explain why the dimerization does not open the spin gap fully but with a size proportional to the Zn-substitution level.

Finally, the current results also bring in an interesting connection to the possibility of experimental realization of the long sought resonant valence bond (RVB) state. For a zigzag spin-chain system, it has been shown that the RVB state is the exact ground state at the ratio of $J_2/J_1=-1/4$.[49] Since

Fig. 9 shows that J_1 remains nearly invariant while J_2 decreases with the increasing Zn, one might view our system is actually approaching this RVB critical point at high Zn level, i.e., Zn level higher than ~5.5% is near the onset of the RVB state. The RVB state on a finite spin chain due to spinless Zn substitution has gapped low-lying excitations which give rise to a cusp shaped susceptibility as indicated in Fig. 5(b). Clearly more theoretical exploration is necessary when interchain coupling and easy-plane anisotropy are considered.

IV. CONCLUSIONS

In conclusion, we have used nonmagnetic Zn substitution to explore the quantum quasi-two-dimensional helimagnet $LiCu_2O_2$. Zn substitution moves the frustrated spin system closer to the quantum-critical ferromagnetic boundary near $\alpha=-1/4$ on the J_2 vs J_1 phase diagram. Two kinds of magnetic orderings have been found crossing the T-z phase boundary for z near ~5.5% per CuO_2 chain. Low Zn substitution reduces the spiral ordering transition temperatures significantly, following a finite-size scaling law, which implies the existence of two-dimensional helimagnetic domains confined by isolated spins, and these isolated spins could be transported as a soliton through the frustrating spin background to the domain boundaries. Such spin phase separation is uniquely observed in a two-dimensional helimagnetic background. High Zn substitution introduces a gapped phase that shows spin-Peierls character and that the phase fraction is proportional to the Zn-substitution level. The proposed interpretations on phase separation, spin dimerization, and spin freezing require more microscopic experimental evidences and muon spin-resonance investigation of the title compound is under way.

ACKNOWLEDGMENTS

F.C.C. acknowledges the support from National Science Council of Taiwan under Project No. NSC-98-2119-M-002-021. The work at McMaster was supported by NSERC, CFI, and CIFAR.

*fcchou@ntu.edu.tw

[1] S. Park, Y. J. Choi, C. L. Zhang, and S.-W. Cheong, Phys. Rev. Lett. **98**, 057601 (2007).
[2] H. Katsura, N. Nagaosa, and A. V. Balatsky, Phys. Rev. Lett. **95**, 057205 (2005).
[3] S. Seki, Y. Yamasaki, M. Soda, M. Matsuura, K. Hirota, and Y. Tokura, Phys. Rev. Lett. **100**, 127201 (2008).
[4] T. Masuda, A. Zheludev, A. Bush, M. Markina, and A. Vasiliev, Phys. Rev. Lett. **92**, 177201 (2004).
[5] C. Fang, T. Datta, and J. Hu, Phys. Rev. B **79**, 014107 (2009).
[6] L. Mihály, B. Dóra, A. Ványolos, H. Berger, and L. Forró, Phys. Rev. Lett. **97**, 067206 (2006).
[7] A. S. Moskvin, Yu. D. Panov, and S.-L. Drechsler, Phys. Rev. B **79**, 104112 (2009).
[8] A. A. Gippius, E. N. Morozova, A. S. Moskvin, A. V. Zalessky, A. A. Bush, M. Baenitz, H. Rosner, and S.-L. Drechsler, Phys. Rev. B **70**, 020406(R) (2004).
[9] T. Masuda, A. Zheludev, B. Roessli, A. Bush, M. Markina, and A. Vasiliev, Phys. Rev. B **72**, 014405 (2005).
[10] R. Berger, A. Meetsma, S. van Smaalen, and M. Sundberg, J. Less Common Met. **175**, 119 (1991).
[11] Y. Yasui, K. Sato, Y. Kobayashi, and M. Sato, J. Phys. Soc. Jpn. **78**, 084720 (2009).
[12] S. W. Huang, D. J. Huang, J. Okamoto, C. Y. Mou, W. B. Wu, K. W. Yeh, C. L. Chen, M. K. Wu, H. C. Hsu, F. C. Chou, and C. T. Chen, Phys. Rev. Lett. **101**, 077205 (2008).
[13] H. C. Hsu, H. L. Liu, and F. C. Chou, Phys. Rev. B **78**, 212401 (2008).
[14] A. M. Vorotynov, A. I. Pankrats, G. A. Petrakovski, K. A. Sablina, W. Paszkowicz, and H. Szymczak, Sov. Phys. JETP **86**, 1020 (1998).
[15] F. C. Fritschij, H. B. Brom, and R. Berger, Solid State Commun. **107**, 719 (1998).
[16] Y. Mizuno, T. Tohyama, S. Maekawa, T. Osafune, N. Motoyama, H. Eisaki, and S. Uchida, Phys. Rev. B **57**, 5326 (1998).
[17] T. Kimura, Y. Sekio, H. Nakamura, T. Siegrist, and A. P. Ramirez, Nature Mater. **7**, 291 (2008).
[18] R. Berger, P. Önnerud, and R. Tellgren, J. Alloys Compd. **184**, 315 (1992).
[19] S.-L. Drechsler, J. Málek, J. Richter, A. S. Moskvin, A. A. Gippius, and H. Rosner, Phys. Rev. Lett. **94**, 039705 (2005).
[20] V. V. Mazurenko, S. L. Skornyakov, A. V. Kozhevnikov, F. Mila, and V. I. Anisimov, Phys. Rev. B **75**, 224408 (2007).
[21] H. Bethe, Z. Phys. **71**, 205 (1931).
[22] M. Enderle, C. Mukherjee, B. Fåk, R. K. Kremer, J.-M. Broto, H. Rosner, S.-L. Drechsler, J. Richter, J. Malek, A. Prokofiev, W. Assmus, S. Pujol, J.-L. Raggazzoni, H. Rakoto, M. Rheinstädter, and H. M. Rønnow, Europhys. Lett. **70**, 237 (2005).
[23] S.-L. Drechsler, O. Volkova, A. N. Vasiliev, N. Tristan, J. Richter, M. Schmitt, H. Rosner, J. Málek, R. Klingeler, A. A. Zvyagin, and B. Büchner, Phys. Rev. Lett. **98**, 077202 (2007).
[24] R. Bursill, G. A. Gehring, D. J. J. Farnell, J. B. Parkinson, T. Xiang, and C. Zeng, J. Phys.: Condens. Matter **7**, 8605 (1995).
[25] K. Okamoto and K. Nomura, Phys. Lett. A **169**, 433 (1992).
[26] M. Schmitt, J. Málek, S.-L. Drechsler, and H. Rosner, Phys. Rev. B **80**, 205111 (2009).
[27] C.-W. Liu, S. Liu, Y.-J. Kao, A. L. Chernyshev, and A. W. Sandvik, Phys. Rev. Lett. **102**, 167201 (2009).
[28] S. B. Oseroff, S.-W. Cheong, B. Aktas, M. F. Hundley, Z. Fisk, and L. W. Rupp, Jr., Phys. Rev. Lett. **74**, 1450 (1995).
[29] M. Hase, K. Uchinokura, R. J. Birgeneau, K. Hirota, and G. Shirane, J. Phys. Soc. Jpn. **65**, 1392 (1996).
[30] H. Fukuyama, T. Tanimoto, and M. Saito, J. Phys. Soc. Jpn. **65**, 1182 (1996).
[31] K. M. Kojima, Y. Fudamoto, M. Larkin, G. M. Luke, J. Merrin, B. Nachumi, Y. J. Uemura, M. Hase, Y. Sasago, K. Uchinokura, Y. Ajiro, A. Revcolevschi, and J.-P. Renard, Phys. Rev. Lett. **79**, 503 (1997).
[32] H. C. Hsu, W. L. Lee, J.-Y. Lin, H. L. Liu, and F. C. Chou, Phys. Rev. B **81**, 212407 (2010).

[33] R. D. Shannon, Acta Crystallogr., Sect. A: Cryst. Phys., Diffr., Theor. Gen. Crystallogr. **32**, 751 (1976).
[34] J. Bobroff, N. Laflorencie, L. K. Alexander, A. V. Mahajan, B. Koteswararao, and P. Mendels, Phys. Rev. Lett. **103**, 047201 (2009).
[35] M. Hase, I. Terasaki, Y. Sasago, K. Uchinokura, and H. Obara, Phys. Rev. Lett. **71**, 4059 (1993).
[36] L. N. Bulaevskii, A. I. Buzdin, and D. I. Khomskii, Solid State Commun. **27**, 5 (1978).
[37] M. E. Fisher and M. N. Barber, Phys. Rev. Lett. **28**, 1516 (1972).
[38] J. H. Cho, F. C. Chou, and D. C. Johnston, Phys. Rev. Lett. **70**, 222 (1993).
[39] A. Bühler, N. Elstner, and G. S. Uhrig, Eur. Phys. J. B **16**, 475 (2000).
[40] J. W. Johnson, D. C. Johnston, A. J. Jacobson, and J. F. Brody, J. Am. Chem. Soc. **106**, 8123 (1984).
[41] N. Laflorencie and D. Poilblanc, Jpn. J. Appl. Phys., Suppl. **74**, 277 (2005).
[42] N. Laflorencie and D. Poilblanc, Phys. Rev. Lett. **90**, 157202 (2003).
[43] S. Furukawa, M. Sato, Y. Saiga, and S. Onoda, J. Phys. Soc. Jpn. **77**, 123712 (2008).
[44] C. K. Majumdar and D. K. Ghosh, J. Math. Phys. **10**, 1388 (1969).
[45] E. Dagotto, Science **309**, 257 (2005).
[46] T. Kimura, T. Goto, H. Shintani, K. Ishizaka, T. Arima, and Y. Tokura, Nature (London) **426**, 55 (2003).
[47] Y. Naito, K. Sato, Y. Yasui, Y. Kobayashi, Y. Kobayashi, and M. Sato, J. Phys. Soc. Jpn. **76**, 023708 (2007).
[48] S. Furukawa, M. Sato, and S. Onoda, arXiv:1003.3940 (unpublished).
[49] T. Hamada, J. Kane, S. Nakagawa, and Y. Natsume, J. Phys. Soc. Jpn. **57**, 1891 (1988).